2024

REPOLARIZING TUMOR-ASSOCIATED MACROPHAGES IN OVARIAN CANCER: A NOVEL IMMUNOTHERAPEUTIC APPROACH

David Schweer
University of Kentucky, dssc224@uky.edu
Author ORCID Identifier:
https://orcid.org/ 0000-0001-7706-5206
Digital Object Identifier: https://doi.org/10.13023/etd.2024.309

STUDENT AGREEMENT:

I represent that my thesis or dissertation and abstract are my original work. Proper attribution has been given to all outside sources. I understand that I am solely responsible for obtaining any needed copyright permissions. I have obtained needed written permission statement(s) from the owner(s) of each third-party copyrighted matter to be included in my work, allowing electronic distribution (if such use is not permitted by the fair use doctrine) which will be submitted to UKnowledge as Additional File.

I hereby grant to The University of Kentucky and its agents the irrevocable, non-exclusive, and royalty-free license to archive and make accessible my work in whole or in part in all forms of media, now or hereafter known. I agree that the document mentioned above may be made available immediately for worldwide access unless an embargo applies.

I retain all other ownership rights to the copyright of my work. I also retain the right to use in future works (such as articles or books) all or part of my work. I understand that I am free to register the copyright to my work.

REVIEW, APPROVAL AND ACCEPTANCE

The document mentioned above has been reviewed and accepted by the student's advisor, on behalf of the advisory committee, and by the Director of Graduate Studies (DGS), on behalf of the program; we verify that this is the final, approved version of the student's thesis including all changes required by the advisory committee. The undersigned agree to abide by the statements above.

David Schweer, Student

Dr. Jill Kolesar, Major Professor

Dr. Claire Clark, Director of Graduate Studies

REPOLARIZING TUMOR-ASSOCIATED MACROPHAGES IN OVARIAN CANCER: A NOVEL IMMUNOTHERAPEUTIC APPROACH

DISSERTATION

A dissertation submitted in partial fulfillment of the
requirements for the degree of Doctor of Philosophy in the
College of Medicine
at the University of Kentucky

By
David Steven Schweer
Lexington, Kentucky
Director: Dr. Jill M Kolesar, Professor of Pharmacy
Lexington, Kentucky
2024

https://orcid.org/0000-0001-7706-520

ABSTRACT OF DISSERTATION

REPOLARIZING TUMOR-ASSOCIATED MACROPHAGES IN OVARIAN CANCER: A NOVEL IMMUNOTHERAPEUTIC APPROACH

Ovarian cancer, recognized for its high lethality and resistance to conventional immunotherapies, mandates innovative strategies to confront its intricate challenges. The tumor microenvironment (TME), orchestrated by tumor-associated macrophages (TAMs), assumes a pivotal role in disease progression, rendering TAMs an appealing therapeutic target. This study endeavors to explore the prospect of repolarizing TAMs from a protumor M2 phenotype to an antitumor M1 state, employing M1 macrophage-derived vesicles (MEVs) as a groundbreaking immunotherapeutic approach.

The primary objective is to investigate the capacity of M1 MEVs to repolarize M2 macrophages in vitro towards an anti-tumor M1-like phenotype. By inducing human macrophages to adopt an M1 phenotype and generating MEVs, the study seeks to uncover their potential to reshape the immunosuppressive TME towards a more favorable antitumor state.

Concurrently, the research addresses the crucial issue of cancer-targeting properties for selective chemotherapy delivery, utilizing cisplatin-encapsulated MEVs (cisMEVs). This dual-focused approach aims to enhance therapeutic precision while mitigating off-target effects, imperative for overcoming prevalent resistance mechanisms in ovarian cancer. The comprehensive assessments of cisMEVs encompass cell viability, dsDNA damage, and TAM repolarization, providing a nuanced understanding of their multifaceted impact on the complex ovarian cancer microenvironment.

Additionally, the study evaluates the in vivo localization of murine-derived M1 MEVs within ovarian cancer tumor xenografts. The promising outcomes in both in vitro and in vivo settings underscore the potential clinical significance of MEVs in redefining the ovarian cancer therapeutic landscape.

In conclusion, this study unveils the potential of MEVs as an innovative and multifunctional avenue for ovarian cancer immunotherapy. By repolarizing TAMs and enhancing cancer cell targeting, MEVs offer a promising strategy to navigate the challenges posed by the immunosuppressive TME in ovarian cancer, paving the way for future therapeutic advancements and improved patient outcomes.

KEYWORDS: Ovarian cancer, Tumor-associated macrophages, M1 Macrophages, M2 Macrophages, Vesicles, Immunotherapy

David Steven Schweer
(Name of Student)

06/01/2024
Date

REPOLARIZING TUMOR-ASSOCIATED MACROPHAGES IN OVARIAN CANCER: A NOVEL IMMUNOTHERAPEUTIC APPROACH

By
David Steven Schweer

Dr. Jill M Kolesar
Director of Dissertation

Dr. Claire Clark
Director of Graduate Studies

06/01/2024
Date

To my beloved wife, Christina

ACKNOWLEDGMENTS

The following dissertation, while an individual work, benefited from the insights and direction of several people. First, my Dissertation Chair, Jill Kolesar, PharmD, MS who, exemplifies the high quality scholarship to which I aspire. In addition, Dr. Kolesar provided timely and instructive comments and evaluation at every stage of the dissertation process, allowing me to complete this project on schedule. Next, I wish to thank the complete Dissertation Committee, and outside reader, respectively: Frederick R. Ueland, MD, Thomas H. Kelly, PhD, Christopher Richards, PhD, and Alexander H. Flannery, PharmD, PhD. Each individual provided insights that guided and challenged my thinking, substantially improving the finished product.

I would also like to thank the members of Dr. Kolesar's and Dr. Richard's lab whose technical and instrumental assistance was critical to the success of the project: J. Robert McCorkle PhD, Kristen S. Hill, PhD, Abigail M. Anderson, PhD, Namrata Anand, PhD, Alexandra N. Nail, PhD, Khaga R. Neupane, PhD, and Brock Harvey. Additionally, I would like to thank my clinical faculty for their support and guidance with my clinical and surgical training: Frederick Ueland, MD, Charles Dietrich, MD, Lauren Baldwin, MD, Rachel Miller, MD, Tricia Fredericks, MD, Christopher DeSimone, MD, and Holly Gallion, MD. I received equally important assistance from my co-fellows during my training here at the University of Kentucky: L. Mackenzie Harbin, MD, Taylor Rives, MD, Megan Hutchcraft, MD, Connie Cao, MD, Allison Swiecki-Sikora, MD, McKayla Riggs, MD, Justin Gorski, MD, PhD, and Anthony McDowell, MD. I would also like to recognize my parents, L. Gregory Schweer and Maryann E. Schweer for their support and guidance during my education. Finally, I would like to thank and acknowledge my

wonderful and loving wife, Dr. Christina Rios, for her support and faith during my training and research. Without her support and belief, this would not have been possible.

TABLE OF CONTENTS

LIST OF FIGURES

CHAPTER 1. INTRODUCTION

1.1 Background

Ovarian cancer is the leading cause of death in gynecological cancers. The American Cancer Society estimates that in 2024 there will be 19,680 new cases of ovarian cancer and 12,740 deaths [1]. Most patients are diagnosed at an advanced stage, with a 5-year survival rate of less than 50% [2]. Patients with advanced-stage ovarian cancer are treated with combination platinum and taxane chemotherapy in the front-line setting. While many patients initially show a response to chemotherapy, the majority will ultimately relapse [2, 3]. Unlike other solid tumors, immunotherapy has been largely ineffective in ovarian cancer [4, 5], emphasizing the need for novel immunotherapies to treat this disease.

1.2 Tumor-associated macrophages

Recent research suggests that tumor-supportive tumor-associated macrophages (TAMs) promote tumor vascularization and metastasis and are predominantly anti-inflammatory, M2-like macrophages [6, 7]. In contrast, pro-inflammatory, M1-like macrophages can clear cancer cells and are associated with a better prognosis [8-10]. A recent meta-analysis demonstrated that high numbers of TAMs are negatively associated with overall survival in multiple solid tumor types, including ovarian cancer [11]. As macrophages are highly plastic, an area of growing interest is the repolarization of anti-inflammatory TAMs to pro-inflammatory TAMs as a potential mechanism of increasing the sensitivity of cancer cells to multiple therapies, including immunotherapy.

Approaches to initiate macrophage repolarization include small molecule

inhibitors, in vitro-transcribed mRNA, toll-like receptor (TLR) agonists, and siRNAs delivered via nanoparticles, all of which have demonstrated repolarization of M2-like TAMs to a M1 phenotype, resulting in downregulation of pro-tumor markers, such as vascular endothelial growth factor (VEGF) and transforming growth factor-beta (TGF-β), and upregulation of pro-inflammatory markers, including tumor necrosis factor-alpha (TNF-α) and interferon-γ (IFN-γ). However, the aforementioned approaches are limited because they fail to localize to tumor associated cells, and therefore heighten the potential for off-target side effects [7, 12-14]. Additional approaches include increasing the antibody-dependent cell-mediated cytotoxicity (ADCC) of TAMs utilizing low-fucosylated antibodies, such as humanized glyco-engineered anti-AMHRII monoclonal antibody murlentamab, holds potential promise, via stimulating an antitumor adaptive immune response via TAM repolarization [15].

1.3 Vesicle therapy

Interest in using vesicles as potential therapeutics has grown significantly in recent years [16]. Vesicles are structures of varying sizes that are created endogenously by cells and they can also be bioengineered by several techniques. In biological systems, vesicles enable cell-to-cell communication, via the transfer of proteins, lipids, and nucleic acids [17, 18]. As a therapeutic modality, vesicles can encapsulate various therapeutic agents, while minimizing immunogenicity and can efficiently target the same cell type as the donor cell [16, 19, 20]. This targeting property has led to the investigation of endogenous vesicles, exosomes, isolated from cancer cells to target comparable primary malignant cells [21, 22]. Currently, there is limited data on the role of cancer cell exosomes to specifically target ovarian cancer. One study examined exosomes from

SKOV3 ovarian cancer cells, subsequently loaded with triptolide, an antineoplastic agent, and demonstrated anti-tumor efficacy in ovarian cancer models [23]. Yet, it should be noted there are significant theoretical and practical concerns with the utilization of exosomes derived from cancer cells as prior studies have suggested that tumor cell exosomes may enhance tumor progression and metastasis [17, 21, 22, 24-31].

Another approach is the utilization of vesicles derived from macrophages to target the macrophage-abundant tumor microenvironment seen in ovarian cancer [32]. M1-type exosomes from RAW 264.7 cells, a murine macrophage line, can polarize unstimulated RAW 264.7 macrophages to the M1 phenotype [33]. However, exosomes are limited in their therapeutic use due to low production yields and limitations in loading drug cargo. An alternative approach that has recently shown promise is bioengineering vesicles from macrophage cell membranes. These macrophages engineered vesicles (MEVs) can be formed by rupturing the cell membrane into fragments via nitrogen cavitation and allowing them to reconstitute into smaller distinct vesicle units. Engineered vesicles derived from the mouse RAW 264.7 cell line show similar properties as macrophage exosomes and can be loaded with a broad range of cargo, including therapeutics [34, 35].

1.4 Macrophage engineered vesicles

MEVs derived from M1 macrophages can serve dual purposes; they can be used as a novel delivery vector for chemotherapeutics and can immunomodulate TAMs [35-37]. Prior studies have demonstrated that mouse-derived M1 MEVs can repolarize mouse M2 macrophages back to an M1 state in vitro [35, 36]. In addition, mouse M1 MEVs can be loaded with platinum-chemotherapeutics and have in vitro anti-cancer activity [36].

Additional studies have shown that macrophage-derived vesicles loaded with paclitaxel have anti-cancer effects against multidrug-resistant cancer cell lines and murine breast cancer models [38, 39].

1.5 Overview

Here we describe the generation of MEVs from human peripheral blood mononuclear cells (PBMCs) that have been differentiated into macrophages. This is an advancement in our prior work by utilizing primary non-tumor human cells from fresh primary isolations [35, 36]. We show that human M1 MEVs localize to both human macrophages and cancer cells and can repolarize M2 macrophages to an M1 phenotype. Human M1 MEVs display anticancer effects in co-culture with ovarian cancer cells. Cisplatin-loaded MEVs display enhanced cytotoxicity compared to free drug. Additionally, using ovarian xenografts in mice, we demonstrate localization of RAW264.7 M1 MEVs to ovarian tumors in vivo.

CHAPTER 2. MATERIALS AND METHODS

2.1 Cell lines

The ovarian adenocarcinoma cell lines: Caov-3, OVCAR3, and SKOV3 along with the murine macrophage line: RAW264.7, were obtained from ATCC. Caov-3 cells and RAW264.7 cells were maintained in Dulbecco's Modified Eagle's Medium (DMEM, ATCC), supplemented with 10% fetal bovine serum (FBS, Sigma). OVCAR3 cells were maintained in RPMI-1640 medium with glutamine and glucose (ATCC), supplemented with 10mg/mL insulin from bovine pancreas (Sigma) and 20% fetal bovine serum (FBS, Sigma). SKOV3 cells were maintained in McCoy's 5a Medium Modified (ATCC), supplemented with 10% fetal bovine serum (FBS, Sigma). Cells were maintained at 37˚C with 5% CO_2.

2.2 Human PBMC isolation and differentiation

Human PBMCs were isolated from buffy coats from 4-5 healthy donors (Kentucky Blood Center, Lexington, KY) by density gradient centrifugation (Ficoll-Paque Premium, GE Healthcare, Sweden) for each preparation of MEVs. Monocytes were isolated from PBMCs by immunomagnetic negative selection (EasySep Human Monocyte Enrichment Kit, Stemcell Technologies, Cambridge, MA). Human PBMC-derived monocytes were cultured in RPMI-1640 (ATCC) with 10% heat-inactivated Fetal Bovine Serum (Sigma-Aldrich, St. Louis, MO), 1% penicillin-streptomycin (Gibco), and recombinant human macrophage colony-stimulating factor (M-CSF, 50ng/mL, PeproTech, Rocky Hill, NJ) for 5-6 days. Media was replaced every 48 hours. M0 macrophages were stimulated for 24 hours with lipopolysaccharide (LPS, 20ng/mL,

Invivogen) plus recombinant human interferon-γ (IFN-γ, 20ng/mL, PeproTech) for M1 macrophages or with recombinant human interleukin-4 (IL-4, 20ng/mL, PeproTech) plus recombinant human interleukin-13 (IL-13, 20ng/mL, PeproTech) for M2 macrophages. Cells were maintained at 37°C with 5% CO_2.

2.3 Vesicle generation and characterization

M1 MEVs were generated from human M1 macrophages using nitrogen (N_2) cavitation. Cells were washed to remove any remaining cytokines, manually disrupted from cell flasks using a cell scraper, and then resuspended in phosphate-buffered saline (VWR) plus protease inhibitor (Thermo Scientific). N_2 cavitation was performed by maintaining cells in a pre-chilled pressurized chamber (Parr Instruments Company, IL, USA) at 250 psi for 5 minutes at 4 ˚C. Vesicles were purified from cellular debris by centrifugation at 4 ˚C for 20 minutes at 4,000 x *g* then 10,000 x *g*. The supernatant was then withdrawn and ultracentrifuged at 100,000 x *g* for 1 hour at 4 ˚C. The subsequent pellet was washed five times with PBS and resuspended in PBS. Cisplatin-loaded human M1 MEVs were generated as described above, with the addition that the N_2 cavitation step was performed in an 8.33 mM solution of cisplatin in PBS. Fluorescein-loaded human M1 MEVs were generated as described above, with the addition that the N_2 cavitation step was performed in a 1mM solution of fluorescein in PBS. For the complete removal of free dye, a diluted vesicle suspension was subjected to an additional ultracentrifugation step at 100,000 x *g* for 60 minutes at 4 °C. The mean diameter, concentration, and zeta potential values of MEVs were obtained via particle tracking analysis using a Zeta View PMX-120 using MEVs generated from $3.1x10^7$ human M1

macrophages**.** Nanoparticle tracking analysis was performed on human M1 MEVs generated from $2.8x10^7$ human M1 macrophages to determine the vesicle size distribution and concentration (NanoSight 300, Malvern Panalytical, United Kingdom).

2.4 Vesicle electron microscopy

The suspended sample of MEVs was fixed with 4% paraformaldehyde for 1 hour and rinsed with 1X PBS. The sample was serially dehydrated with different concentrations of ethanol from 30, 50, 70, 75, 80, 90, 95, 100 and 100% for 10 minutes. A droplet of the sample was pipetted and deposited onto a glass cover slip previously treated with 0.1% solution of poly-L-lysine[1] to promote adhesion. Before the sample could fully dry, it was briefly immersed in ethanol (200 proof) and transferred into a critical point dryer (EM CPD 300, Leica Microsystems, Wetzlar, Germany) system. After drying, the surface of the sample was metallized by sputter coating 5 nm of platinum (EM ACE 600, Leica Microsystems, Wetzlar, Germany) to enhance surface electrical conductivity and subsequently imaged using a field-emission scanning electron microscope (SEM, Quanta 250 FEG, ThermoFisher Scientific, formerly FEI, Hillsboro, OR, USA).

SKOV3 cells were incubated with M1 vesicles for 24 hours. After incubation, the cells were washed with PBS and fixed with 4% paraformaldehyde for 40 minutes at room temperature (RT). The cells were then processed for immunogold labelled silver enhancement stain (IGSS). Cells were blocked with 3% BSA for 2 hours and then incubated with monoclonal rabbit anti-human CD86 (1:250 dilution) overnight at 4^0C. Cells were then incubated with secondary anti-rabbit IgG Alexa Fluor® 647 Fluoro

Nanogold (Nanoprobes) at 1:100 dilution for 2 hours at RT. Silver enhancement was performed using HQ silver enhancement kit (Nanoprobes) for 5 minutes at RT. The cells were then washed three times with deionized water and further incubated with 0.2% osmium tetraoxide in PBS at 4˚C for 1 hour. Cell samples were exposed with 0.25% uranyl acetate for 1 hour at 4^0C to preserve the immunogold labelling. Samples were then dehydrated using serial concentrations of ethanol: 50%, 70%, 90% and 100% (three times). Samples were then embedded with 100% resin. Samples were washed with resin twice, with the second wash added to samples and incubated for 45-60 minutes in a 60^0C oven. A final resin polymerization was performed for 48 hours at 60^0 C. Cultured cells were then separated from plates and a 100nm section was cut with a microtome and mounted on FCF-200-Cu grids. Images were acquired using a Thermo Scientific™ Talos™ F200X TEM [40].

2.5 Imaging of Fluorescently-Labeled Vesicles

Fluorescein-labeled vesicles were generated as discussed previously and fixed onto a glass-bottom dish before imaging using a fluorescence microscope. Fluorescein-loaded vesicles were imaged using a 488 nm laser of 0.8 mW power and an exposure time of 200 ms.

2.6 Cytokine analysis

Human PBMC-derived monocytes were plated in 24-well plates at 1 x 10^6 cells/well and cultured with M-CSF (50 ng/mL) for six days. Cells were stimulated in duplicate to M1 or M2 macrophages as previously described. M1 macrophages from the

same PBMC isolation plated on separate plates were used to generate MEVs. Vesicles were washed to remove any remaining cytokines, then plated with M2 macrophages. Media supernatants were collected following a 24-hour incubation period and were assayed in duplicate using a human TNF-α Quantikine ELISA kit (R&D Systems, Inc., Minneapolis, MN). Optical density was measured using a microplate reader (Varioskan LUX, Thermo Scientific, Finland). Experiments were performed in triplicate.

2.7 Real-time PCR of macrophage biomarkers.

Human peripheral blood monocytes were isolated, plated, and cultured for five days into differentiated M0 macrophages. M0 macrophages were plated in a 6-well plate at a concentration of 5.0×10^5 per well, after which macrophages were polarized to either an M1 or M2 state using LPS/IFNγ or IL4/IL13, respectively. M1 MEVs were prepared from additional M1 macrophages as previously described and were then used to treat M2 macrophages. Following an additional 24-hour incubation, RNA was purified from human macrophages (M0, M1, M2, MEV-treated M2) with RNeasy Plus Universal Mini Kit (Qiagen), and 500 ng of each sample was converted to cDNA using High-Capacity cDNA Reverse Transcription Kit (ThermoFisher Scientific) with random primers. TaqMan Advanced Master Mix with TaqMan Gene Expression Assays (ThermoFisher Scientific were used to measure gene expression via real-time semi-quantitative PCR. Expression of human CXCL8 (assay ID Hs00174103_m1), CXCL10 (assay ID Hs00171042_m1), relative to endogenous control GAPDH (assay ID Hs02758991_g1) were measured in triplicate using a QuantStudio 3 Real-Time PCR instrument (Applied

Biosystems). Relative expression was evaluated across samples with QuantStudio Software (Applied Biosystems) using the Comparative C_T ($\Delta\Delta C_T$) method.

2.8 Co-culture of human M2 macrophages and cancer cells

For co-culture imaging experiments, human M0 macrophages were plated at 5 x 10^4 cells/well in a 96-well clear-bottom, black-walled plate. M0 cells were stimulated to M1 or M2 for 24 hours. Caov-3 ovarian adenocarcinoma cells (ATCC) were then plated at 5000 cells/well with M1 or M2 macrophages. Human M1 MEVs were generated and labeled with a lipophilic dialkylcarbocyanine fluorescent dye, DiI (1,1'-Dioctadecyl-3,3,3',3'-Tetramethylindocarbocyanine Perchlorate, Molecular Probes Inc., Invitrogen, Eugene, OR). DiI labeled vesicles were obtained by incubating MEV-resuspension with 5 μM DiI for 30 minutes at 37 °C. The free dye molecules were separated from the fluorescently-labeled vesicles using a size exclusion spin column (PD MidiTrap column) following the manufacturer's protocol. Human M1 DiI-labeled MEVs at a 10% dilution were added to Caov-3 cells, M2 macrophages, or Caov-3 plus M2 macrophage co-culture. After a 24-hour incubation period, cells were imaged at 40x with confocal microscopy (CellInsight CX7 High-Content Screening Platform). Cells were incubated with Hoescht (1:2000) for 30 minutes before imaging to label nuclei.

For cell viability experiments, human M0 macrophages were plated at 2.5-5 x 10^4 cells/well in a 96-well plate. M0 cells were stimulated to M1 or M2 for 24 hours. Supernatant was then removed and Caov-3 ovarian adenocarcinoma cells (ATCC) were then plated at 5000 cells/well with M1 or M2 macrophages. M0, M1, and M2 macrophages and Caov-3 controls were each plated in at least duplicate. Supernatants

were collected after 24 hours. 20% or 10% dilution of human M1 MEVS was added to Caov-3 cells only and Caov-3 plus M2 cells in duplicate. Supernatants were collected after 24-hour incubation with MEVs, and wells were replaced with complete media. A cell viability assay was performed after 96 hours following the addition of MEVs according to the manufacturer's instructions (CellTiter-Glo 2.0, Promega). Luminescence was measured with a microplate reader (Varioskan LUX). This process was repeated in the same manner with OVCAR3 cells. Experiments for both cell lines were performed in triplicate. The collected supernatants were assayed in duplicate using a human TNF-α Quantikine ELISA kit (R&D Systems, Inc., Minneapolis, MN).

2.9 Cisplatin loaded human MEV dose response curves

Ovarian cancer cells (Caov-3, SKOV3, OVCAR3) were plated at 5 x 10^3 cells/well in a 96-well plate and incubated at 37˚C for 24 hours. Human macrophages were generated and cultured as previously noted. Vesicles were generated using nitrogen cavitation (300psi) in a 8.33mM cisplatin solution (or PBS for unloaded vesicles). Cisplatin-loaded MEVs were prepared by making serial dilutions in media to 12 concentrations from 20% MEVs to 0.0098% MEVs. The concentration of drug in cisplatin-loaded MEVs was calculated using mass spectrometry analysis. Free cisplatin was prepared by making serial dilutions of cisplatin in media, 12 concentrations of free cisplatin were plated in duplicate on cells, ranging from 100uM - 0.0006uM. Drug free media was plated with cells as a control. A cell viability assay was performed after 72 hours following the addition of MEVs according to manufacturer's instructions (CellTiter-Glo 2.0, Promega). Luminescence was measured with a microplate reader

(Varioskan LUX). Dose response curves and the IC50 were calculated using combined triplicate values in GraphPad Prism 5. Statistical significance was calculated using a one-tailed paired t-test on separate paired experimental IC50s (GraphPad Prism 5). All experiments were performed in triplicate.

2.10 CX7 γ-H2AX staining DNA damage assay

Ovarian cancer cells (Caov-3, OVCAR3, SKOV3) were seeded 5x103 cells per well of black-walled, clear-bottom 96-well plates (ThermoFisher Scientific) in 100μL complete growth media. Cells were allowed to attach overnight at 37° C with 5% CO_2. Human macrophages generated and cultured as previously noted. Vesicles were generated using nitrogen cavitation (300psi) in a 8.33mM cisplatin solution (or PBS for unloaded vesicles). Media was then removed and replaced with media containing serial dilutions of cisMEVs (20-0.08%), 10-5μm cisplatin (positive control), or respective cell media. Cells were incubated another 48 hours at 37° C with 5% CO_2. Following treatment, cells were fixed for 15 minutes at room temperature with 4% paraformaldehyde, permeabilized for 15 minutes at room temperature with 0.25% Triton X-100 and blocked for 1 hour at room temperature with 0.1% (w/v) bovine serum albumin in D-PBS. Nuclei were labeled with Hoechst 33258 and double-strand DNA breaks were assessed using the HCS DNA Damage Kit (Invitrogen), with a primary antibody targeting phosphorylated histone H2AX (γH2AX) and an AlexaFluor 555-conjugated secondary antibody. Cells were imaged with the CellInsight CX7 High Content Analysis Platform (ThermoFisher Scientific) and nuclear γH2AX was quantified using HCS Studio software (ThermoFisher Scientific). Signal intensities were normalized

to vehicle-treated control and expressed as fold-change relative to control. Signal differences were analyzed using GraphPad Prism 5. One-way analysis of variance and Tukey's multiple comparison tests were used to determine if treatment-induced fold-change in γH2AX signal within each cell line was significantly different from vehicle-treated control cells. The concentration of drug in cisplatin-loaded MEVs was calculated using mass spectrometry analysis. The cisMEV groups with the most comparable cisplatin concentration to the positive control were analyzed using one-sided t-tests (GraphPad Prism 5) Experiments were performed in triplicate.

2.11 Murine tumor pathology and staining.

Caov-3 human ovarian cancer cells were transduced with luciferase-expression vector (pLL-CMV-rFLuc-T2A-GFP-mPGK-Puro) using lentivirus (MOI=15) and grown in the presence of 500 ng/mL puromycin. Luciferase-positive cells ($5x10^6$) were injected intraperitoneally in 6-week old female nude mice. Mice were injected with XenoLight D-Luciferin K+ salt (PerkinElmer) at 150 mg/kg body weight and imaged for bioluminescence using IVIS Spectrum In Vivo Imaging System (PerkinElmer). Eight weeks after tumor cell inoculation, xenograft tumor tissue was harvested, fixed in 10% formalin and embedded in paraffin. Tissue was sectioned and stained with standard hematoxylin and eosin (H&E) and antibodies specific for human epithelial cells: EPCAM (Abcam) and mouse macrophages: F4/80 (Abcam) and CD68 (LSBio) for immunohistochemistry.

2.12 RAW264.7 MEV generation and mouse localization experiments:

RAW264.7 cells were maintained at 37 °C with 5% CO_2. RAW264.7 cells were stimulated to an M1 state using LPS/ IFNγ at a concentration of 20 ng/ml for 24 hours. Cells were then manually collected using a cell scraper, and vesicles were generated in the same manner as described above. The vesicle pellet was resuspended in 2 ml of sucrose buffer (10 mM HEPES, 250 mM Sucrose pH 7.5). DiR ($DiIC_{18}(7)$; 1,1′-dioctadecyl-3,3,3′,3′-tetramethylindotricarbocyanine iodide) (ThermoFisher Scientific) was utilized as a lipophilic fluorescent dye, with 5 µl of 2 mM added to the vesicle solution and then incubated for 30 minutes at 37 °C. The vesicle solution was then layered with a 50% and 10% OptiPrep™ density gradient medium. The combined solution was then ultracentrifuged at 112,000 x g for 60 minutes at 4 °C. A peristaltic pump was then used to collect DiR labeled vesicles between the gradients. The collected vesicles were purified using size exclusion PD Miditrap columns (Cytiva) to remove any free dye.

Under the University of Kentucky Institutional Animal Care & Use Committee (IACUC) protocol #2017-2674, we did a transperitoneal injection of 5-week-old female BALB/c SCID mice (Jackson Lab) with 5 x 10^6 Caov-3 cells in 100 µl of sterile PBS. After visible tumor progression, 100-200ul of labeled RAW264.7 MEVs were injected via lateral tail veins of via intraperitoneal injection in the right lower quadrant. Athymic nude homozygous 5-week-old female (Jackson Lab) were subcutaneously injected with 2.5-5.0 x 10^6 SKOV3 cells in 100ul of sterile PBS in the dorsal shoulder region. Mice were imaged 72 hours post-injection using a LagoX Small Animal Optical Imager (Spectral Instruments) at a fluorescent excitation wavelength of 710 nm and emission of

770 nm for 10 seconds. Images were processed with Aura Imaging software (Spectral Instruments). After euthanasia, necropsy performed with tumor and organs of interest isolated and imaged independently.

CHAPTER 3. RESULTS

3.1 Characterization of human MEVs

MEVs are formed via mechanical disruption of macrophage cell membranes with nitrogen cavitation [35]. The generated cellular fragments subsequently reform into vesicles in a pressurized chamber. To determine the ability of human MEVs to encapsulate cargo, human MEVs were generated in the presence of fluorescein, a fluorescent dye. MEVs were imaged using a fluorescence microscope using a 488 nm laser of 0.8 mW power with a gain of 990 and an exposure time of 200 ms. MEVs were visible as bright punctate regions (Fig. 1A). This illustrates that human MEVs can encapsulate cargo during vesicle generation, similar to MEVs generated from RAW 264.7 cells [35]. To characterize the vesicle size distribution within an individual preparation of MEVs, we quantified the vesicle diameter and concentration using multiple particle tracking using a Zeta View PMX-120 (Fig 1B) and Nanosight 300 (Fig. 1C-D). We generated vesicles from 3.1 x 10^7 human M1 macrophages with a cavitation pressure of 250 psi, which yielded 6.6 x 10^{10} vesicles with a mean diameter of 125.1 nm (SD ± 60.2 nm). Additionally, we measured the Zeta potential at -127mV; a large negative value is an indicator of stability in an aqueous solution. Additional characterization performed with Nanosight 300 (Fig. 1C-E) using 2.8 x 10^7 human M1 macrophages yielding 6.45x10^{11} with a mean diameter of 165.1nm (SD ± 66.4nm).

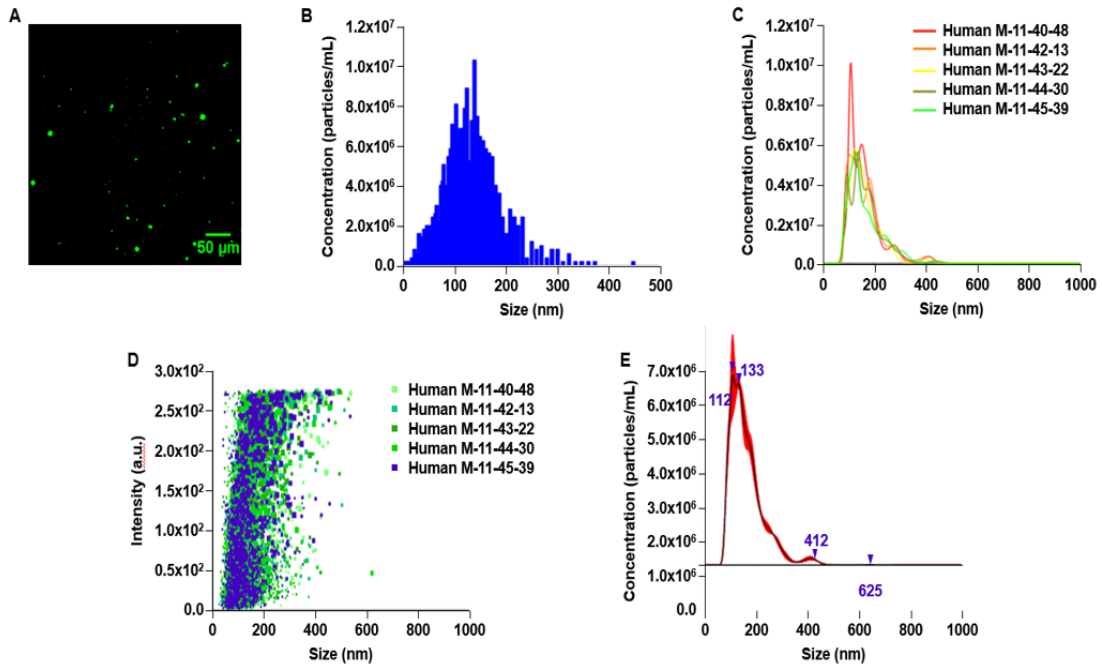

Figure 1. Characterization of human PMBC-derived M1 vesicles

Scanning electron microscopy (SEM) was performed in order to determine the shape and morphology of the generated MEVs. MEVs were fixed and serially dehydrated prior to SEM. Examination confirmed the round smooth-edged morphology with diameter of a single MEV of~200nm (Fig 2A). The dense MEV spherical morphology suggests a tendency to encapsulate the cargo drug with firm stability. Utilizing transmission electron microscopy (TEM), M1 vesicles were then identified using CD86 monoclonal antibody. CD86 is a known glycoprotein found in the membrane of the antigen presenting cells, such as blood monocytes and macrophages. Fig 2B shows positive immunogold staining of M1 MEVs (positive for CD86) as seen as dark black silver particles within a SKOV3 cell. The SKOV3 cell membrane and nucleus containing chromatin were also visible.

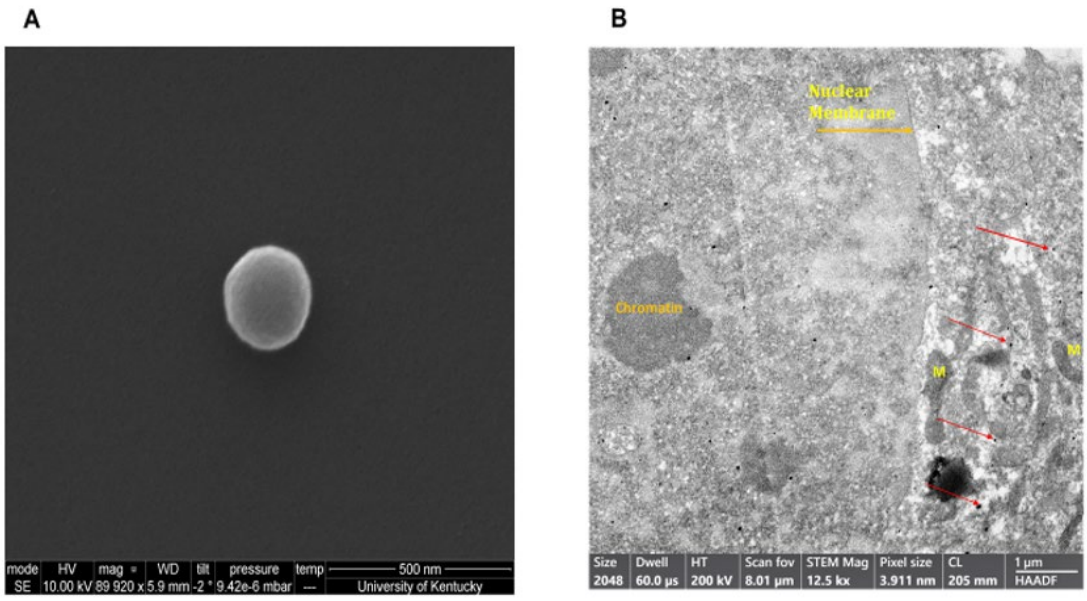

Figure 2. Scanning electron microscopy vesicle imaging

3.2 M1 MEVs are taken up by M2 macrophages and cancer cells

Next, we examined if M1 MEVs can localize to M2 macrophages and ovarian carcinoma cells. We generated M1 MEVs labeled with DiI, a lipophilic fluorescent dye that is loaded in the membrane. MEVs were incubated with M2 macrophages, Caov-3 cells, and co-culture of M2 macrophages plus Caov-3 cells. Confocal imaging with a CellInsight CX7 High-Content Screening Platform demonstrated that both human M2 macrophages and Caov-3 cells uptake MEVs in co-culture (Fig. 3A). Caov-3 cells and macrophages demonstrated different nuclear sizes when cocultured alone, with Caov-3 nuclei significantly larger. (Fig. 3B). While Caov-3 cells showed a low level of punctate MEVs co-localizing to the cells, most macrophages, indicated by smaller nuclei, display a distinctly higher number of MEVs (Fig. 3C). These results show that human MEVs are capable of localizing to both human macrophages and human ovarian cancer cells in

vitro.

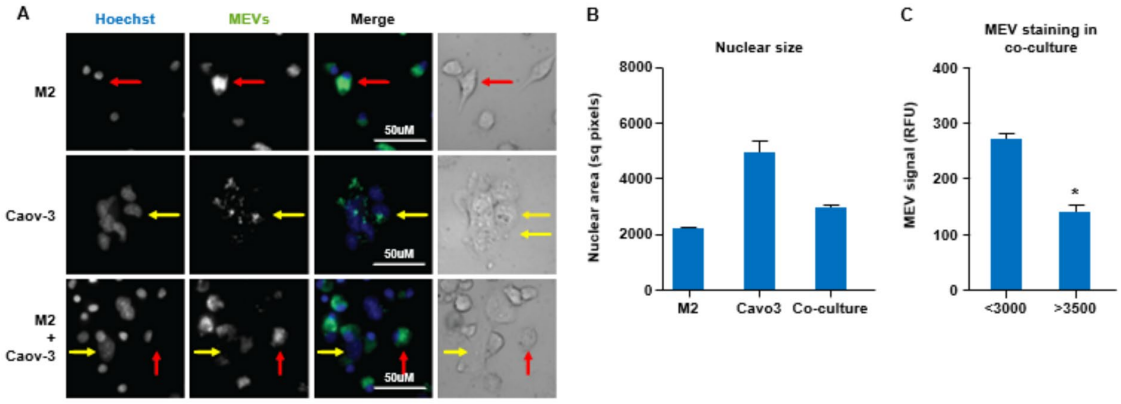

Figure 3. Human macrophage display a higher uptake of human M1 MEVs compared to ovarian cancer cells

3.3 M1 MEVs repolarize M2 macrophages

Next, we tested if human M1 MEVs can repolarize M2 macrophages to an M1-like, pro-inflammatory phenotype. We compared the production of the pro-inflammatory cytokine TNF-α in M1 macrophages, M2 macrophages, and M2 macrophages incubated with M1 MEVs. We observed high levels of TNF-α, measured via ELISA, in the M1 macrophages and significantly lower TNF-α in the M2 culture and in controls (Mean ± SD pg/ml: M1 vs. M2: 2021 ± 383.8 vs. 259.9 ± 133.7, $p<0.001$, M1 MEVs+M2 vs. M2: 787.5 ± 298.3 vs. 259.9 ± 133.7 $p<0.05$) (Fig. 4a). In contrast, we observed an increase in TNF-α in M2 macrophages that were incubated with M1 MEVs, indicating that M1 MEVs can repolarize M2 macrophages towards a pro-inflammatory, M1-like macrophage phenotype. Figure 4b demonstrates the difference in TNF- α levels of M1+M1 MEVs vs M1 cells alone is not significant. However, M2+ M1 MEVs vs M2 cells is statistically significant. From this data we've concluded that the MEVs alone are not the sole driver of the experimental increased TNF-α levels, but rather the interaction with the M2 cells

via repolarization. The comparatively lower TNF-α levels seen in the M1 between Fig 4A & B is likely secondary to the difference in analyzed time points (24 vs 48 hrs) and experimental methodology. We subsequently sought to validate M1 MEV repolarization of M2 macrophages via real-time PCR of mRNA expression of CXCL8 and CXCL10 proteins. Figure 4c shows significant differences in the relative expression of CXCL8 in M2 cells alone compared to M2 cells treated with M1 MEVs ($p<0.0001$). This finding was not demonstrated in relative mRNA expression of CXCL10 (Fig 4d). CXCL8 expression is marker for M1 macrophages [41-43]. Therefore, based on CXCL8 mRNA expression, M1 MEVs can repolarize M2 to an M1 state. Taken together, M1 MEVs can repolarize M2 macrophages into an M1-like phenotype based on both cytokine secretion and mRNA expression profiles.

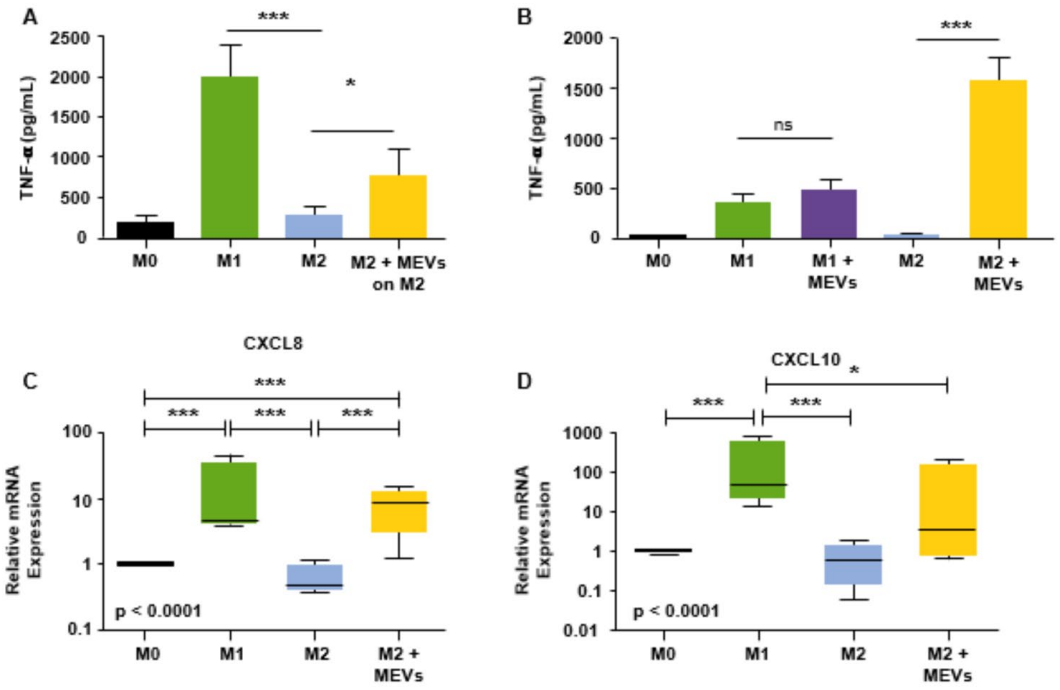

Figure 4. Human PMBC-derived M1 vesicles repolarize M2 macrophages

3.4 Human M1 MEVs repolarize M2 macrophages in co-culture

To test if M1 MEVs can convert M2 TAMs to a pro-inflammatory phenotype, we cultured human M2 macrophages with the Caov-3 or OVCAR3 ovarian cancer cell lines and treated the co-cultured cells with M1 MEVs. Co-cultured cells treated with M1 MEVs show an increase in the pro-inflammatory cytokine, TNF-α (Mean ± SD pg/ml: M2+Caov-3+M1 MEVs vs M2+Caov-3; 383.6 ± 120.4 vs. 0.1389 ± 20.03, $p<0.05$, M2+OVCAR3+M1 MEVs vs M2+OVCAR3: 207.1±170.2 vs -45.65±55.35 p=0.18) (Fig. 5a & d), suggesting that M1 MEVs convert M2 TAMs to an M1 phenotype. The comparatively lower TNF-α levels seen in the M1 plus cancer cells (Fig. 5A & D) compared to the high levels of TNF-α in the M1 macrophages alone (Fig 4) is likely secondary to the difference in time points (24 vs 48 hrs) and experimental methodology.

We then tested if M1 MEVs are capable of inhibiting cell viability. M1 MEVs at high concentrations has an inhibitory effect in both Caov-3 (Mean ± SD 100.0 ± 8.232 vs 82.27± 2.853, $p<0.0001$) and OVCAR3 cell lines (Mean ± SD 100.0 ± 5.710 vs 87.69± 11.62, $p<0.05$) (Fig 5B & E), with continued significant decreases appreciated at a lower dose (10%) in Caov-3 (Mean ± SD: 100.0 ± 8.232 vs 87.95± 6.069, $p<0.0001$). Interestingly, in Caov-3 this inhibition appears to be dose-dependent and is significantly higher in the co-cultured cells as compared to cancer cells alone (Mean ± SD 100.0 ± 2.930 vs. 70.54 ± 9.955, $p<0.0001$) (Fig. 5C), indicating that MEVs are more effective in the presence of pro-inflammatory macrophages. The inhibition seen in OVCAR3 cells co-cultured with M2 macrophages is more modest but still significant at a high MEV dose (Mean ± SD 100.0± 6.821 vs 93.61 ± 5.558, $p < 0.01$) (Fig 5F).

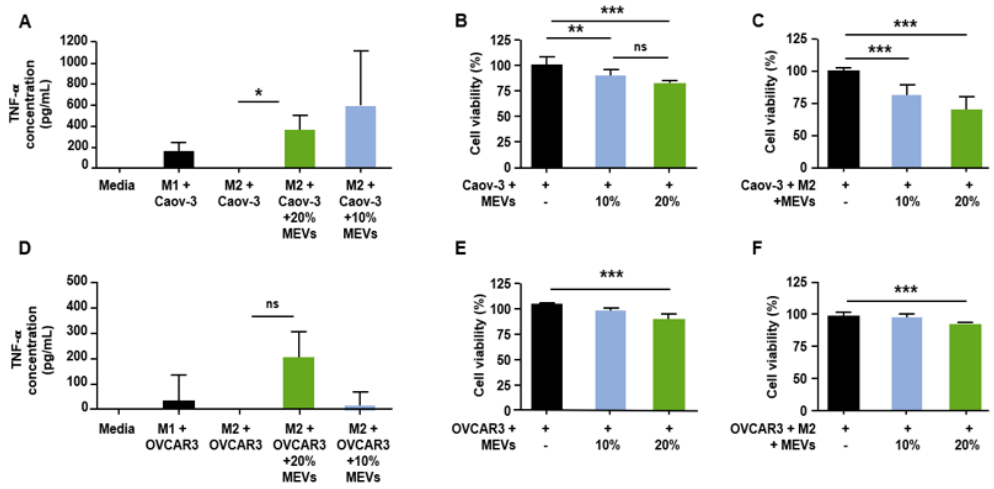

Figure 5. Human M1 MEVs repolarize M2 macrophages in co-culture

3.5 Cisplatin-loaded vesicles retain cytotoxicity in-vitro at lower concentrations than free cisplatin

Compared to free cisplatin, cisMEVs demonstrate statistically significant enhanced inhibition of proliferation in Caov-3 (IC50: 1.262 µM, 95%CI:1.105-1.442 vs 5.734 µM 95%CI: 5.015- 6.556; p=0.0447) (Figure 6) and approached significance in OVCAR3 (2.398 µM, 95%CI: 2.233 - 2.574 vs 3.686 µM, 95%CI: 3.061 - 4.438; p= 0.0772) (Figure 7) and SKOV3 (1.927 µM, 95%CI: 1.544 - 2.406 vs 4.707 µM, 95%CI: 3.080 - 7.192; p= 0.1079) (Figure 8).

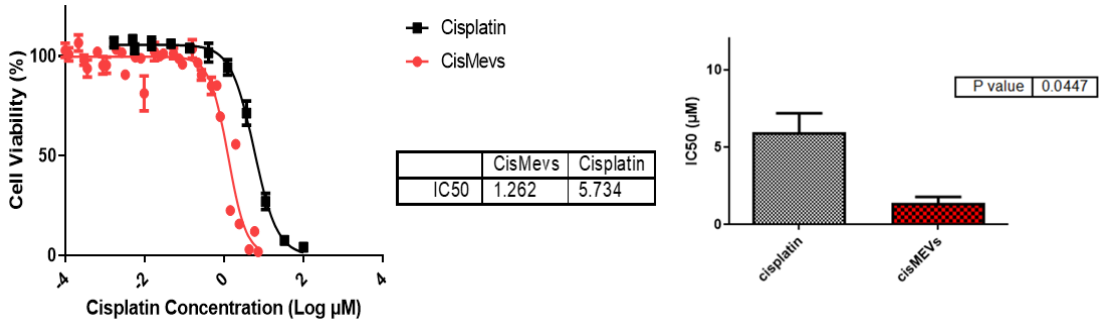

Figure 6. Caov-3 dose-response cisplatin loaded MEVs

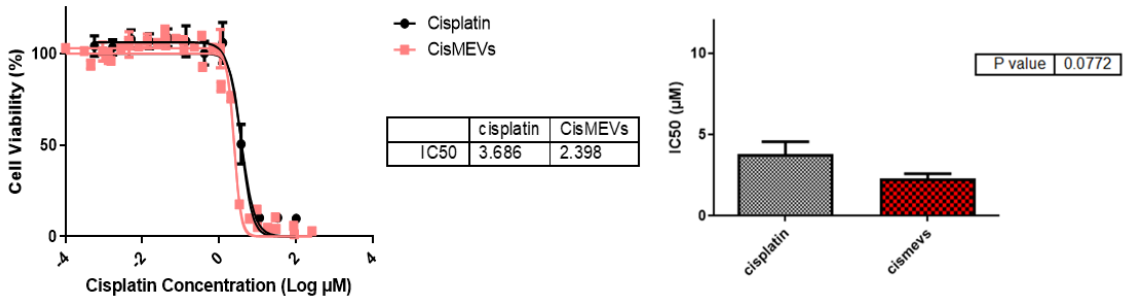

Figure 7. OVCAR3 dose-response cisplatin loaded MEVs

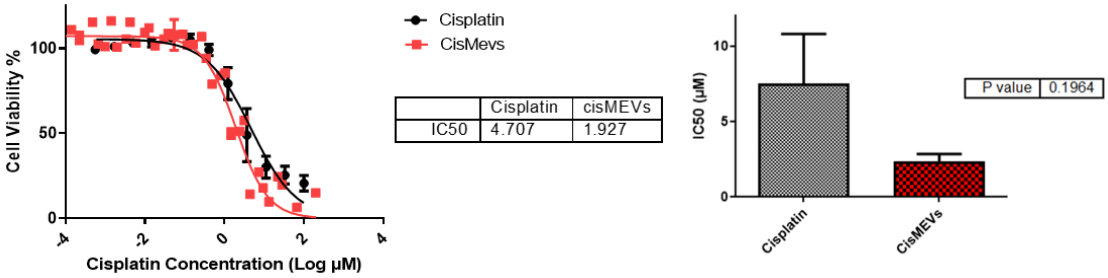

Figure 8. SKOV3 dose-response cisplatin loaded MEVs

In regards to dsDNA damage assays utilizing a γ-H2AX staining levels, one-ANOVA results demonstrated significant differences in γ-H2AX signal across titration groups in Caov-3 ($p<0.0001$) (Figure 9), OVCAR3($p<0.0001$) (Figure 10), and SKOV3

(p=0.0002) (Figure 11). Full analysis results with Tukey's method for multiple comparison results are available in Appendix 1.

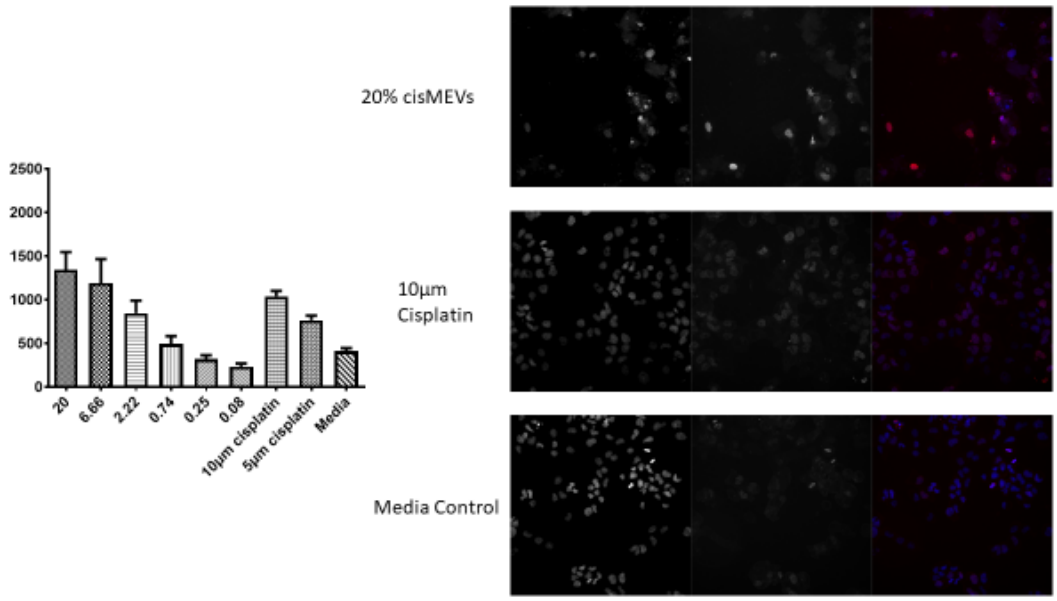

Figure 9. Caov-3 cisMEV γ-H2AX signal dose response

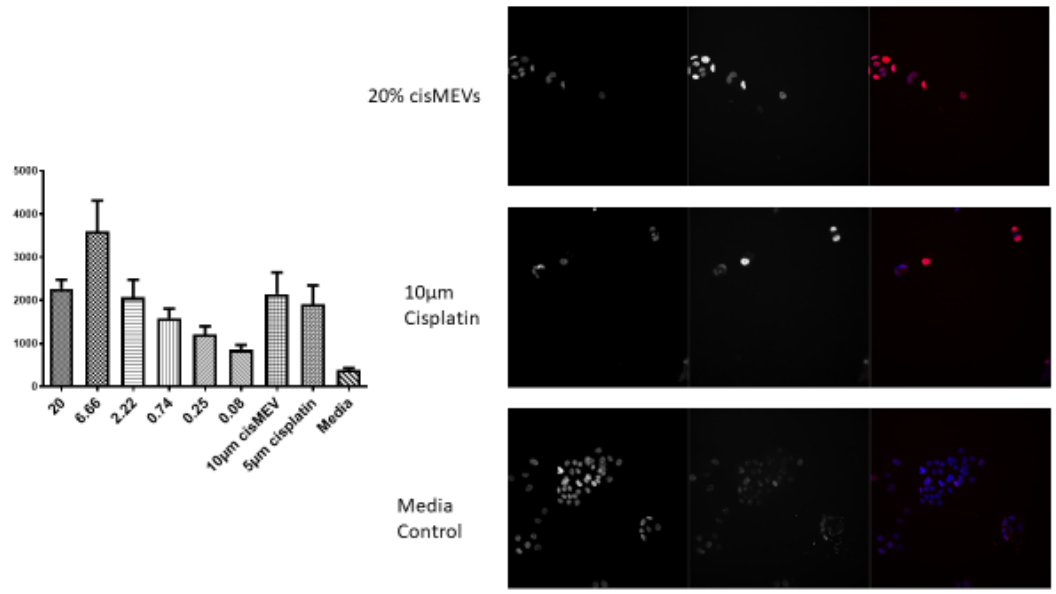

Figure 10. OVCAR3 cisMEV γ-H2AX signal dose response

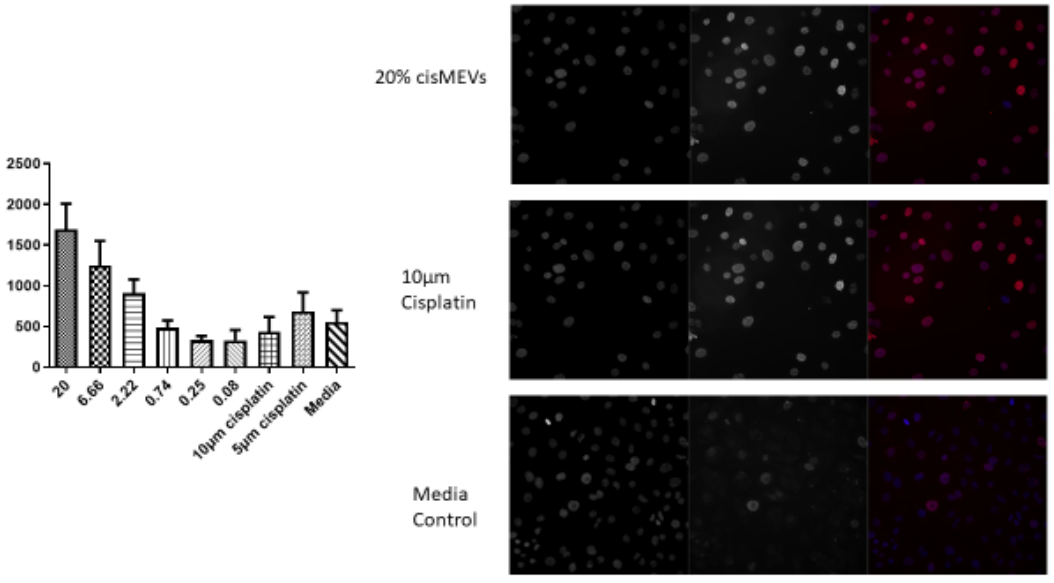

Figure 11. SKOV3 cisMEV γ-H2AX signal dose response

When comparing cisMEV concentrations of 3.9uM (average dose retrospectively determined via LC/MS) to free cisplatin concentrations of 5uM, cisMEVs demonstrated

statistically significant differences in fold change in Caov-3 (Mean fold change ± SE cisMEV vs cisplatin: 2.812 ± 0.3154 vs 1.876 ± 0.06574, p=0.0012) (Figure 12) and OVCAR3 (Mean fold change± SE cisMEV vs cisplatin: 10.34 ± 2.613 vs 4.386 ± 0.4013, p=0.0046) (Figure 13), but not significant in SKOV3 (Mean fold change ± SE cisMEV vs cisplatin: 5.097 ± 1.009 vs 4.302 ± 0.3408 p=0.1996) (Figure 14).

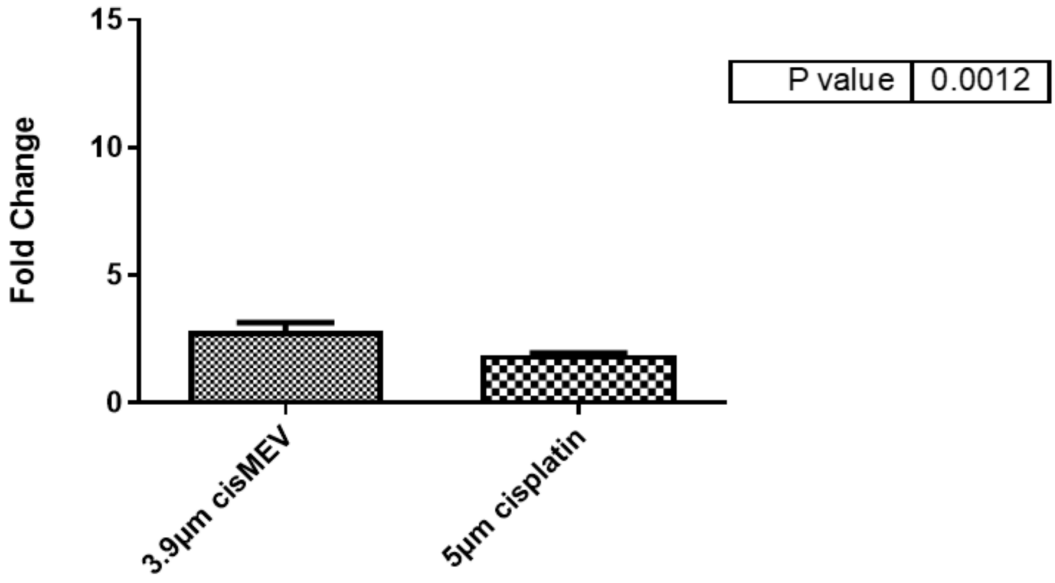

Figure 12. Caov-3 cisMEV γ-H2AX signal fold change

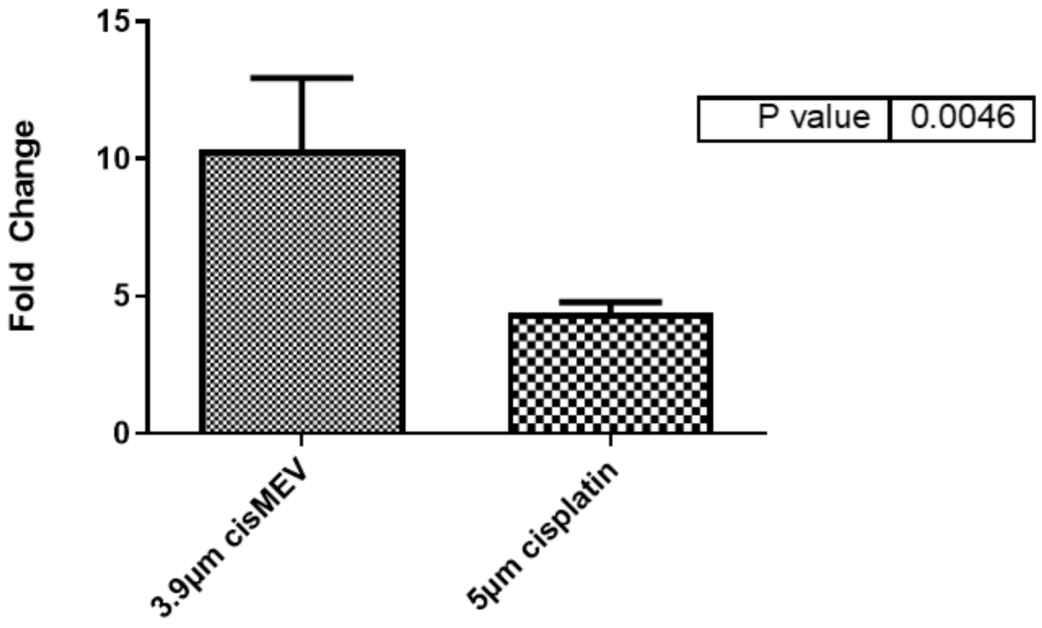

Figure 13. OVCAR3 γ-H2AX signal fold change

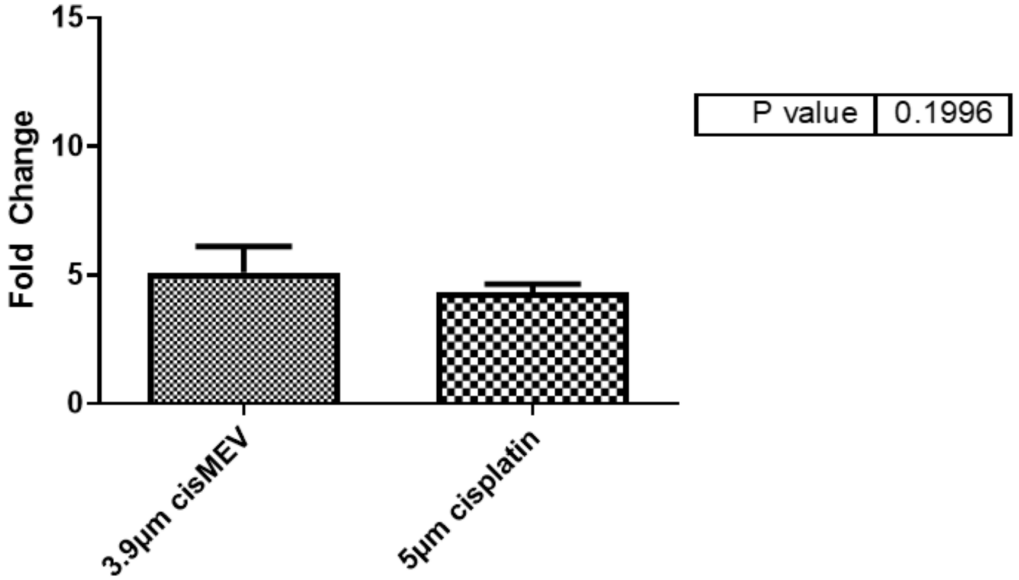

Figure 14. SKOV3 γ-H2AX signal fold change

3.6 RAW264.7-derived M1 MEVs localize to ovarian xenografts in vivo.

Murine tumors harvested from Caov-3 innoculated nude mice (Figure 15A), stained positive for EPCAM, a human epithelial marker, indicating a tumor consistent with a human ovarian epithelial primary (Figure 15B). Additional immunohistochemistry stains with F4/80 and CD68, demonstrate macrophage infiltration into the tumors (Figure 15 C&D).

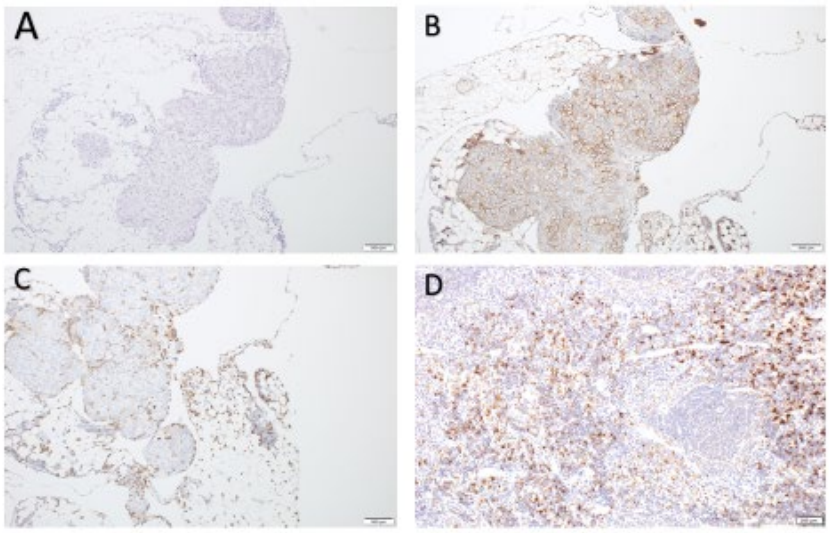

Figure 15. Mouse Caov-3 tumor xenograft

As part of a pilot experiment, we sought to demonstrate the localization of M1 MEVs to human tumor xenografts. A BALB/c SCID mouse was injected transperitoneally with Caov-3 ovarian cancer cells and developed a visible tumor xenograft in the abdominal right lower quadrant approximately seven months post-injection. Fluorescent DiR-labelled M1 MEVs were created from RAW264.7 cells and were injected via lateral tail vein. Importantly, RAW264.7 are a mouse macrophages cell

line. The mouse was imaged 72hrs post-injection (Fig 16) using appropriate corresponding emission and excitation wavelengths for DiR. An additional mouse (left) without a tumor xenograft was not injected was imaged for baseline null comparison purposes. The dye-labeled MEVs demonstrate precise localization to the tumor (Fig 16. B&C). Additional pilot experiments were performed with athymic nude mice injected subcutaneously with SKOV3 ovarian cancer cells xenografts in the mouse scapular region. Fluorescent DiR-labelled M1 MEVs were created from RAW264.7 cells and were injected via lateral tail vein (Fig 17) or intraperitoneally (Fig 18). Post-necropsy images demonstrate localization of M1 MEVs to tumor (Figure 17E). Intermittent fluorescent signalling demonstrated in the murine cranium at 24 hours is noted, but desists at 72hours. This is suggestive of a transient circulatory phenomenon or may reflect additional M2 macrophage target populations.

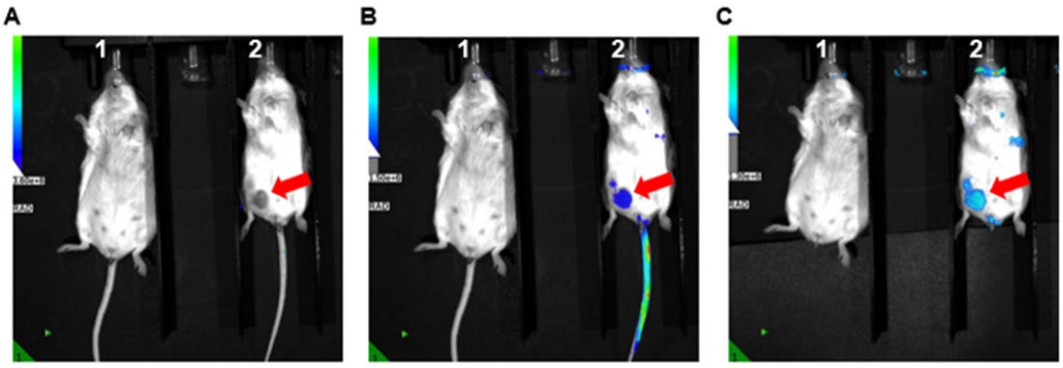

Figure 16. Caov-3 mouse xenograft RAW264.7 vesicle localization

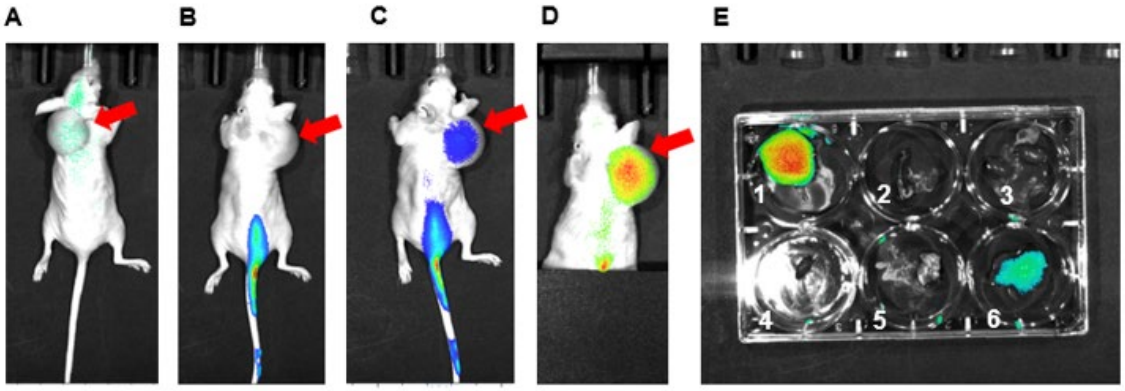

Figure 17. SKOV3 mouse intravenous RAW264.7 vesicle localization

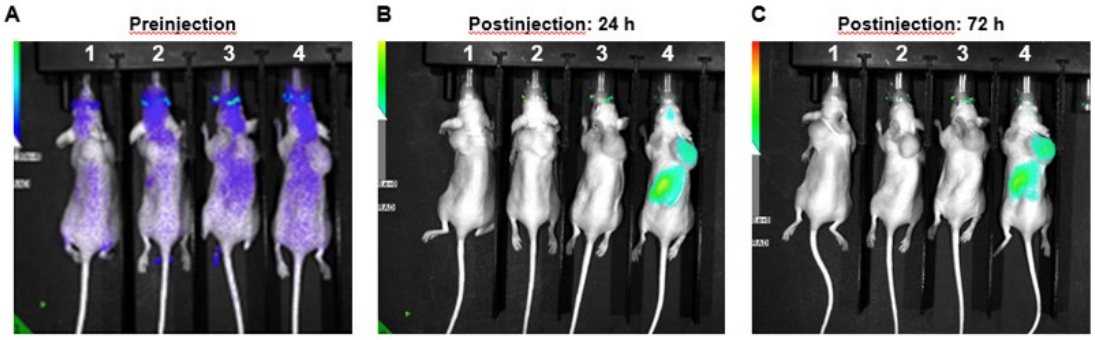

Figure 18. SKOV3 xenograft intraperitoneal RAW264.7 vesicle localization

CHAPTER 4. DISCUSSION

4.1 Overview

While there have been several recent advances in immunotherapy for other gynecological malignancies (cervical [25] and uterine [26]), success in ovarian cancer has been limited [27]. This lack of activity in ovarian cancer is thought to be related to infiltration of TAMs, which render cancer "cold" and thus immunotherapy ineffective [34, 44]. Therefore, strategies to repolarize M2 macrophages to the M1 phenotype may promote anti-cancer activity. Our study, the first to use MEVs derived from human blood monocytes, effectively demonstrates that M1 MEVs can localize primarily to M2 macrophages when co-cultured with ovarian cancer cells and treatment with M1 MEVs repolarizes M2 macrophages to an anti-tumor M1 state with subsequent anti-cancer activity. This effect was demonstrated both in cancer cells alone and with macrophages co-cultured in the presence of cancer cells. Since ovarian cancer cells themselves are significant drivers for macrophage polarization to an M2 state [45], repolarization within co-culture is particularly salient as it suggests the capacity of MEVs to overcome an innate preferential differentiation towards the protumor M2 state.

Macrophages are the most abundant immune system cells within the tumor microenvironment and compose up to 50% of a tumor's volume [46-48]. A major benefit of exosome formulations from macrophages is the inherent targeting properties exhibited by their origin cell [18]. Exosomes derived from human cells are non-immunogenic compared to liposomal formulation [18]. Therefore, the use of exosome-like MEVs derived from human blood cells has the potential to avoid off-target immunogenic effects while honing in on macrophage-laden tissue (e.g., tumors). Additionally, engineered

macrophage vesicles carry a higher yield potential than other endogenous sources while avoiding a cancer-derived source that could impact tumorigenesis [27, 49, 50].

4.2 Strengths and limitations

One of the main strengths of this study is the exclusive use of non-carcinoma human-derived cells. This eliminates any future translational risk of reintroducing tumor-derived cells into the patient. Another major strength is the immunological and therapeutic potential of M1 MEVs that is demonstrated using several ovarian cancer cell lines. Caov-3 and OVCAR3 are both BRCA wild-type, however, Caov-3 is platinum-sensitive whereas OVCAR3 are platinum resistant. In murine models, SKOV3 is an aggressive platinum resistant cell line that displays rapid xenograft growth. Interestingly, cisplatin-loaded MEVs demonstrate enhanced cytotoxicity at lower cisplatin doses both from IC50 evaluation and mechanistically via γ-H2AX staining, a marker of dsDNA damage. Additionally, pilot animal data demonstrate precise localization of dye-labeled mouse M1 MEVs to ovarian cancer tumor xenografts in mice. This is an intriguing finding and provides further evidence for the tumor precision of MEVs. Localization was seen in both intravenous and intraperitoneal administration routes. This is of compelling interest as ovarian cancer is a peritoneal disease and intraperitoneal chemotherapy has a long-studied role in the treatment of the disease. [51, 52]. Limitations include a lack of in vivo modeling to demonstrate sustained macrophage repolarization. In terms of generalization of in vivo models, SCID and nude mice are particularly immunosuppressed, future modelling using syngeic murine models may more accurately reflect physiologic conditions and reveal the interplay of circulating MEVs with the

immune system targets. Additionally, there was high variability and size heterogeneity seen with the vesicle preparation that may be ameliorated in future studies with further filtration methods. Additional characterization methods of the vesicles via transmission electron microscopy is warranted.

CHAPTER 5. CONCLUSIONS

5.1 Summary

The studies described are the first to demonstrate that human-derived M1 MEVs can serve as immunomodulatory agents by repolarizing M2 macrophages to an M1-like state. This effect was seen in M2 macrophages when cultured alone and in co-culture with ovarian cancer cells. Overall, human-derived M1 MEVs effectively repolarize M2 macrophages. Initial pilot data demonstrates that M1 MEVs target ovarian tumor xenografts. Future in vivo studies investigating targeting and treatment effect are warranted.

5.2 Future directions

While promising as a therapeutic avenue, significant obstacles remain prior to transition from a preclinical to clinical approach, including standardization of MEV characterization, dosing, precision of imaging localization, and delineation of off-target effects. Initial experiments involving cisplatin-loaded MEVs were highly promising by demonstrating cytotoxicity at comparably lower doses than free cisplatin. Future research will be needed to evaluate the role of drug-loaded MEVs as another therapeutic approach and evaluate in vivo efficacy in terms of distribution, toxicity, and tumor response. Expansion of this investigational approach to additional solid tumors is justified, particularly gynecologic cancers that utilize platinum-based chemotherapy.

APPENDIX

ANOVA TUKEY'S MULTIPLE COMPARISON TEST RESULTS

A. CAOV-3

Tukey's Multiple Comparison Test	Mean Diff.	q	Significant? P < 0.05?	Summary	95% CI of diff
20 vs 6.66	153.7	1.282	No	ns	-387.7 to 695.1
20 vs 2.22	497.4	4.149	No	ns	-44.00 to 1039
20 vs 0.74	852.6	7.112	Yes	***	311.2 to 1394
20 vs 0.25	1024	8.537	Yes	***	482.1 to 1565
20 vs 0.08	1108	9.245	Yes	***	567.0 to 1650
20 vs 10um cis	302.5	2.746	No	ns	-195.0 to 800.0
20 vs 5um cis	580.1	5.266	Yes	*	82.60 to 1078
20 vs media	931.6	9.316	Yes	***	480.0 to 1383
6.66 vs 2.22	343.7	2.967	No	ns	-179.4 to 866.7
6.66 vs 0.74	698.9	6.034	Yes	**	175.9 to 1222
6.66 vs 0.25	869.8	7.51	Yes	***	346.7 to 1393
6.66 vs 0.08	954.6	8.242	Yes	***	431.6 to 1478
6.66 vs 10um cis	148.8	1.407	No	ns	-328.7 to 626.2
6.66 vs 5um cis	426.4	4.033	No	ns	-51.08 to 903.8
6.66 vs media	777.8	8.181	Yes	***	348.5 to 1207
2.22 vs 0.74	355.3	3.067	No	ns	-167.8 to 878.3
2.22 vs 0.25	526.1	4.542	Yes	*	3.078 to 1049
2.22 vs 0.08	611	5.275	Yes	*	87.92 to 1134
2.22 vs 10um cis	-194.9	1.843	No	ns	-672.4 to 282.6
2.22 vs 5um cis	82.71	0.7823	No	ns	-394.7 to 560.2
2.22 vs media	434.2	4.566	Yes	*	4.809 to 863.6
0.74 vs 0.25	170.9	1.475	No	ns	-352.2 to 693.9
0.74 vs 0.08	255.7	2.208	No	ns	-267.3 to 778.7
0.74 vs 10um cis	-550.2	5.203	Yes	*	-1028 to -72.69
0.74 vs 5um cis	-272.5	2.578	No	ns	-750.0 to 204.9
0.74 vs media	78.93	0.8301	No	ns	-350.4 to 508.3
0.25 vs 0.08	84.84	0.7325	No	ns	-438.2 to 607.9
0.25 vs 10um cis	-721	6.819	Yes	***	-1198 to -243.6
0.25 vs 5um cis	-443.4	4.194	No	ns	-920.9 to 34.07
0.25 vs media	-91.93	0.9669	No	ns	-521.3 to 337.4
0.08 vs 10um cis	-805.9	7.622	Yes	***	-1283 to -328.4
0.08 vs 5um cis	-528.2	4.996	Yes	*	-1006 to -50.77
0.08 vs media	-176.8	1.859	No	ns	-606.1 to 252.6
10um cis vs 5um cis	277.6	2.936	No	ns	-149.4 to 704.7
10um cis vs media	629.1	7.626	Yes	***	256.6 to 1002
5um cis vs media	351.5	4.261	No	ns	-21.05 to 724.0

B. OVCAR3

Tukey's multiple comparisons test	Mean Diff.	t	Significant? P < 0.05?	Summary	95% CI of diff
20 vs 6.66	-1335	3.467	No	ns	-3068 to 397.8
20 vs 2.22	199.6	0.5007	No	ns	-1594 to 1993
20 vs 0.74	677	1.758	No	ns	-1056 to 2410
20 vs 0.25	1057	2.745	No	ns	-676.0 to 2790
20 vs 0.08	1413	3.671	No	ns	-319.4 to 3146
20 vs 10um cis	125.5	0.357	No	ns	-1456 to 1707
20 vs 5um cis	360.4	1.025	No	ns	-1221 to 1942
20 vs Media	1879	5.975	Yes	**	463.8 to 3294
6.66 vs 2.22	1535	3.85	No	ns	-259.0 to 3328
6.66 vs 0.74	2012	5.226	Yes	*	279.3 to 3745
6.66 vs 0.25	2392	6.212	Yes	**	659.1 to 4125
6.66 vs 0.08	2749	7.138	Yes	****	1016 to 4481
6.66 vs 10um cis	1461	4.155	No	ns	-121.3 to 3042
6.66 vs. 5um cis	1696	4.824	Yes	*	113.6 to 3277
6.66 vs. Media	3214	10.22	Yes	****	1799 to 4629
2.22 vs. 0.74	477.5	1.198	No	ns	-1316 to 2271
2.22 vs. 0.25	857.3	2.151	No	ns	-936.4 to 2651
2.22 vs. 0.08	1214	3.046	No	ns	-579.8 to 3008
2.22 vs. 10um cis	-74.07	0.2022	No	ns	-1722 to 1574
2.22 vs. 5um cis	160.9	0.4392	No	ns	-1487 to 1809
2.22 vs. Media	1679	5.076	Yes	*	190.4 to 3168
0.74 vs. 0.25	379.8	0.9864	No	ns	-1353 to 2113
0.74 vs. 0.08	736.4	1.912	No	ns	-996.5 to 2469
0.74 vs. 10um cis	-551.6	1.569	No	ns	-2133 to 1030
0.74 vs. 5um cis	-316.6	0.9008	No	ns	-1899 to 1265
0.74 vs. Media	1202	3.822	No	ns	-213.3 to 2617
0.25 vs. 0.08	356.6	0.926	No	ns	-1376 to 2089
0.25 vs. 10um cis	-931.4	2.65	No	ns	-2513 to 650.5
0.25 vs. 5um cis	-696.5	1.981	No	ns	-2278 to 885.4
0.25 vs. Media	821.8	2.614	No	ns	-593.1 to 2237
0.08 vs. 10um cis	-1288	3.664	No	ns	-2870 to 293.9
0.08 vs. 5um cis	-1053	2.996	No	ns	-2635 to 528.9
0.08 vs. Media	465.2	1.48	No	ns	-949.6 to 1880
10um cis vs. 5um cis	234.9	0.7472	No	ns	-1180 to 1650
10um cis vs. Media	1753	6.439	Yes	***	527.9 to 2979
5um cis vs. Media	1518	5.576	Yes	**	292.9 to 2744

C. SKOV3

Tukey's Multiple Comparison Test	Mean Diff.	q	Significant? P < 0.05?	Summary	95% CI of diff
20 vs 6.66	445.1	1.966	No	ns	-577.4 to 1468
20 vs 2.22	785.9	3.471	No	ns	-236.6 to 1808
20 vs 0.74	1214	5.36	Yes	**	191.0 to 2236
20 vs 0.25	1363	6.02	Yes	**	340.6 to 2386
20 vs 0.08	1367	6.038	Yes	**	344.6 to 2390
20 vs 10um cis	1261	6.103	Yes	**	328.0 to 2195
20 vs 5um cis	1011	4.804	Yes	*	60.67 to 1961
20 vs media	1142	6.142	Yes	**	302.2 to 1981
6.66 vs 2.22	340.8	1.505	No	ns	-681.6 to 1363
6.66 vs 0.74	768.4	3.394	No	ns	-254.0 to 1791
6.66 vs 0.25	918	4.054	No	ns	-104.5 to 1940
6.66 vs 0.08	922.1	4.072	No	ns	-100.4 to 1945
6.66 vs 10um cis	816.3	3.949	No	ns	-117.1 to 1750
6.66 vs 5um cis	565.8	2.689	No	ns	-384.4 to 1516
6.66 vs media	696.5	3.747	No	ns	-142.9 to 1536
2.22 vs 0.74	427.6	1.889	No	ns	-594.9 to 1450
2.22 vs 0.25	577.2	2.549	No	ns	-445.3 to 1600
2.22 vs 0.08	581.2	2.567	No	ns	-441.3 to 1604
2.22 vs 10um cis	475.5	2.3	No	ns	-457.9 to 1409
2.22 vs 5um cis	225	1.069	No	ns	-725.2 to 1175
2.22 vs media	355.7	1.914	No	ns	-483.7 to 1195
0.74 vs 0.25	149.5	0.6605	No	ns	-872.9 to 1172
0.74 vs 0.08	153.6	0.6784	No	ns	-868.9 to 1176
0.74 vs 10um cis	47.88	0.2317	No	ns	-885.5 to 981.3
0.74 vs 5um cis	-202.6	0.9631	No	ns	-1153 to 747.6
0.74 vs media	-71.93	0.387	No	ns	-911.3 to 767.4
0.25 vs 0.08	4.06	0.01793	No	ns	-1018 to 1027
0.25 vs 10um cis	-101.7	0.4918	No	ns	-1035 to 831.7
0.25 vs 5um cis	-352.2	1.674	No	ns	-1302 to 598.0
0.25 vs media	-221.5	1.192	No	ns	-1061 to 617.9
0.08 vs 10um cis	-105.7	0.5115	No	ns	-1039 to 827.7
0.08 vs 5um cis	-356.2	1.693	No	ns	-1306 to 594.0
0.08 vs media	-225.5	1.213	No	ns	-1065 to 613.8
10um cis vs 5um cis	-250.5	1.325	No	ns	-1104 to 603.1
10um cis vs media	-119.8	0.743	No	ns	-848.0 to 608.4
5um cis vs media	130.7	0.7874	No	ns	-619.0 to 880.4

REFERENCES

1. Siegel, R.L., et al., *Cancer statistics, 2024.* CA Cancer J Clin, 2024. 74(1):p. 12-49.

2. Kathawala, R.J., A. Kudelka, and B. Rigas, *The Chemoprevention of Ovarian Cancer: the Need and the Options.* Curr Pharmacol Rep, 2018. 4(3): p. 250-260.

3. Pujade-Lauraine, E. and P. Combe, *Recurrent ovarian cancer.* Ann Oncol, 2016. 27 Suppl 1: p. i63-i65.

4. Matulonis, U.A., et al., *Antitumor activity and safety of pembrolizumab in patients with advanced recurrent ovarian cancer: results from the phase II KEYNOTE-100 study.* Ann Oncol, 2019. 30(7): p. 1080-1087.

5. Disis, M.L., et al., *Efficacy and Safety of Avelumab for Patients With Recurrent or Refractory Ovarian Cancer: Phase 1b Results From the JAVELIN Solid Tumor Trial.* JAMA Oncol, 2019. 5(3): p. 393-401.

6. Movahedi, K., et al., *Different tumor microenvironments contain functionally distinct subsets of macrophages derived from Ly6C(high) monocytes.* Cancer Res, 2010. 70(14): p. 5728-39.

7. Yin, W., et al., *Remodeling Tumor-Associated Macrophages and Neovascularization Overcomes EGFR(T790M) -Associated Drug Resistance by PD-L1 Nanobody-Mediated Codelivery.* Small, 2018. 14(47): p. e1802372.

8. Petty, A.J. and Y. Yang, *Tumor-associated macrophages: implications in cancer immunotherapy.* Immunotherapy, 2017. 9(3): p. 289-302.

9. Honkanen, T.J., et al., *Prognostic and predictive role of tumour-associated macrophages in HER2 positive breast cancer.* Sci Rep, 2019. 9(1): p. 10961.

10. Macciò, A., et al., *Role of M1-polarized tumor-associated macrophages in the prognosis of advanced ovarian cancer patients.* Sci Rep, 2020. 10(1): p. 6096.

11. Zhang, Q.W., et al., *Prognostic significance of tumor-associated macrophages in solid tumor: a meta-analysis of the literature.* PLoS One, 2012. 7(12): p. e50946.

12. Rodell, C.B., et al., *TLR7/8-agonist-loaded nanoparticles promote the polarization of tumour-associated macrophages to enhance cancer immunotherapy.* Nat Biomed Eng, 2018. 2(8): p. 578-588.

13. Zhang, F., et al., *Genetic programming of macrophages to perform anti-tumor functions using targeted mRNA nanocarriers.* Nat Commun, 2019. 10(1): p. 3974.

14. Xiao, H., et al., *M2-Like Tumor-Associated Macrophage-Targeted Codelivery of STAT6 Inhibitor and IKKbeta siRNA Induces M2-to-M1 Repolarization for Cancer Immunotherapy with Low Immune Side Effects.* ACS Cent Sci, 2020. 6(7): p. 1208-1222.

15. Gyorgy, B., et al., *Therapeutic applications of extracellular vesicles: clinical promise and open questions.* Annu Rev Pharmacol Toxicol, 2015. 55: p. 439-464.

16. Zhang, L. and D. Yu, *Exosomes in cancer development, metastasis, and immunity.* Biochim Biophys Acta Rev Cancer, 2019. 1871(2): p. 455-468.

17. Ha, D., N. Yang, and V. Nadithe, *Exosomes as therapeutic drug carriers and delivery vehicles across biological membranes: current perspectives and future challenges.* Acta Pharm Sin B, 2016. 6(4): p. 287-96.

18. Robbins, P.D. and A.E. Morelli, *Regulation of immune responses by extracellular vesicles.* Nat Rev Immunol, 2014. 14(3): p. 195-208.

19. Cheng, L., Y. Wang, and L. Huang, *Exosomes from M1-Polarized Macrophages Potentiate the Cancer Vaccine by Creating a Pro-inflammatory Microenvironment in the Lymph Node.* Mol Ther, 2017. 25(7): p. 1665-1675.

20. Walker, S., et al., *Extracellular vesicle-based drug delivery systems for cancer treatment.* Theranostics, 2019. 9(26): p. 8001-8017.

21. Shao, J., J. Zaro, and Y. Shen, *Advances in Exosome-Based Drug Delivery and Tumor Targeting: From Tissue Distribution to Intracellular Fate.* Int J Nanomedicine, 2020. 15: p. 9355-9371.

22. Liu, H., et al., *The Effect of Triptolide-Loaded Exosomes on the Proliferation and Apoptosis of Human Ovarian Cancer SKOV3 Cells.* BioMed Research International, 2019. 2019: p. 2595801.

23. Balaj, L., et al., *Tumour microvesicles contain retrotransposon elements and amplified oncogene sequences.* Nat Commun, 2011. 2: p. 180.

24. Bai, S., et al., *Tumor-Derived Exosomes Modulate Primary Site Tumor Metastasis.* Front Cell Dev Biol, 2022. 10: p. 752818.

25. Kosaka, N., et al., *Versatile roles of extracellular vesicles in cancer.* J Clin Invest, 2016. 126(4): p. 1163-72.

26. Vakhshiteh, F., F. Atyabi, and S.N. Ostad, *Mesenchymal stem cell exosomes: a two-edged sword in cancer therapy.* Int J Nanomedicine, 2019. 14: p. 2847-2859.

27. Li, K., et al., *Exosomes play roles in sequential processes of tumor metastasis.* Int J Cancer, 2019. 144(7): p. 1486-1495.

28. Saleem, S.N. and A.B. Abdel-Mageed, *Tumor-derived exosomes in oncogenic reprogramming and cancer progression.* Cell Mol Life Sci, 2015. 72(1): p. 1-10.

29. Tai, Y.L., et al., *Basics and applications of tumor-derived extracellular vesicles.* J Biomed Sci, 2019. 26(1): p. 35.

30. Giusti, I., et al., *Tumor-Derived Extracellular Vesicles Activate Normal Human Fibroblasts to a Cancer-Associated Fibroblast-Like Phenotype, Sustaining a Pro-Tumorigenic Microenvironment.* Front Oncol, 2022. 12: p. 839880.

31. Colvin, E.K., *Tumor-associated macrophages contribute to tumor progression in ovarian cancer.* Front Oncol, 2014. 4: p. 137.

32. Shi, Y., et al., *M1 But Not M0 Extracellular Vesicles Induce Polarization of RAW264.7 Macrophages Via the TLR4-NFkappaB Pathway In Vitro.* Inflammation, 2020. 43(5): p. 1611-1619.

33. Choo, Y.W., et al., *M1 Macrophage-Derived Nanovesicles Potentiate the Anticancer Efficacy of Immune Checkpoint Inhibitors.* ACS Nano, 2018. 12(9): p. 8977-8993.

34. Snell, A.A., et al., *Cell-Derived Vesicles for in Vitro and in Vivo Targeted Therapeutic Delivery.* ACS Omega, 2019. 4(7): p. 12657-12664.

35. Neupane, K.R., et al., *Macrophage-Engineered Vesicles for Therapeutic Delivery and Bidirectional Reprogramming of Immune Cell Polarization.* ACS Omega, 2021. 6(5): p. 3847-3857.

36. Cabeza, L., et al., *Cancer therapy based on extracellular vesicles as drug delivery vehicles.* J Control Release, 2020. 327: p. 296-315.

37. Kim, M.S., et al., *Development of exosome-encapsulated paclitaxel to overcome MDR in cancer cells.* Nanomedicine, 2016. 12(3): p. 655-664.

38. Wang, P., et al., *Exosomes from M1-Polarized Macrophages Enhance Paclitaxel Antitumor Activity by Activating Macrophages-Mediated Inflammation.* Theranostics, 2019. 9(6): p. 1714-1727.

39. Crivelli, S.M., et al., *Function of ceramide transfer protein for biogenesis and sphingolipid composition of extracellular vesicles.* J Extracell Vesicles, 2022. 11(6): p. e12233.

40. Meniailo, M.E., et al., *Interleukin-8 favors pro-inflammatory activity of human monocytes/macrophages.* Int Immunopharmacol, 2018. 56: p. 217-221.

41. Xuan, W., et al., *The chemotaxis of M1 and M2 macrophages is regulated by different chemokines.* J Leukoc Biol, 2015. 97(1): p. 61-9.

42. Tsai, T.H., et al., *Overexpression of GLUT3 promotes metastasis of triple-negative breast cancer by modulating the inflammatory tumor microenvironment.* J Cell Physiol, 2021. 236(6): p. 4669-4680.

43. Anderson, N.R., et al., *Macrophage-Based Approaches for Cancer Immunotherapy.* Cancer Res, 2021. 81(5): p. 1201-1208.

44. Hagemann, T., et al., *Ovarian cancer cells polarize macrophages toward a tumor-associated phenotype.* J Immunol, 2006. 176(8): p. 5023-32.

45. Zhou, K., et al., *Targeting tumor-associated macrophages in the tumor microenvironment.* Oncol Lett, 2020. 20(5): p. 234.

46. Van Overmeire, E., et al., *Mechanisms driving macrophage diversity and specialization in distinct tumor microenvironments and parallelisms with other tissues.* Front Immunol, 2014. 5: p. 127.

47. Kim, J. and J.S. Bae, *Tumor-Associated Macrophages and Neutrophils in Tumor Microenvironment.* Mediators Inflamm, 2016. 2016: p. 6058147.

48. Meng, W., et al., *Prospects and challenges of extracellular vesicle-based drug delivery system: considering cell source.* Drug Deliv, 2020. 27(1): p. 585-598.

49. Kim, H., et al., *Exosomes: Cell-Derived Nanoplatforms for the Delivery of Cancer Therapeutics.* Int J Mol Sci, 2020. 22(1).

50. Armstrong, D.K., et al., *Intraperitoneal cisplatin and paclitaxel in ovarian cancer.* N Engl J Med, 2006. 354(1): p. 34-43.

51. Walker, J.L., et al., *Randomized Trial of Intravenous Versus Intraperitoneal Chemotherapy Plus Bevacizumab in Advanced Ovarian Carcinoma: An NRG Oncology/Gynecologic Oncology Group Study.* J Clin Oncol, 2019. 37(16): p. 1380-1390.

VITA

David Steven Schweer, MD

EDUCATION

Doctor of Philosophy Candidate at University of Kentucky College of Clinical and Translational Science (07/2020 – Present), Thesis Title: Repolarizing Tumor-Associated Macrophages In Ovarian Cancer: A Novel Immunotherapeutic Approach

Gynecologic Oncology Fellowship (7/2020 – Present) at University of Kentucky Markey Cancer Center, Lexington, Kentucky.

Obstetrics and Gynecology Residency (7/2016 – 6/2020) at University of Florida College of Medicine, Gainesville, Florida

Medical Doctorate (08/2012-05/2016) at Virginia Tech Carilion School of Medicine, Roanoke, Virginia

Bachelor of Science (08/2008-05/2012) in Biology at Virginia Commonwealth University, Richmond, Virginia

PROFESSIONAL EXPERIENCES

Society of Gynecologic Oncology (SGO) Membership Committee
Role: Committee Member (3/2023-3/2025)

SGO Minimally Invasive Surgery Academy Workshop
Role: Fellow (11/2023)

Jackson Laboratory Short Course on Experimental Models of Human Cancer
Role: Physician Attendee (08/2020)

University of Florida Housestaff Council
Role: OBGYN Representative (10/2019 – 06/2020)

Gynecology OR Utilization Committee – University of Florida
Role: Resident Physician Committee Member (06/2019-06/2020)

Memorial Sloan Kettering Hospital – Department of Gynecologic Oncology
Role: Brunschwig Visiting Fellow (02/2019)

Surgical Site Infection Prevention Work Group – University of Florida
Role: Resident Physician Committee Member (10/2017-06/2020)

Ob/Gyn Student Interest Group, Virginia Tech Carilion School of Medicine
Role: Co-President (01/2015-05/2016)

Carilion Clinic Orthopaedics Musculoskeletal Education and Research Center
Role: Medical student researcher (06/2013-05/2016)

HONORS & AWARDS

University of Kentucky

T32: Oncology Research Training for Surgeon Scientists Post-Doctoral Fellowship (2020 – 2022) Principal Investigator: B. Mark Evers, T32 CA160003.

University of Florida College of Medicine
Outstanding *Resident* in Gynecologic Oncology *Award (2020)*

University of Florida College of Medicine
Department of OBGYN Golden Apple Teaching Award (2020)

University of Florida College of Medicine
Highest CREOG Award (2019)

Society of American Gastrointestinal and Endoscopic Surgeons Fundamentals of Laparoscopic Surgery Certification (2019)

University of Florida Shands Hospital
Customer Service is Key Award (2019)

Virginia Tech Carilion School of Medicine
Letter(s) of Distinction: Clinical Science Integration; Radiology *(2016)*

Virginia Commonwealth University
Magna Cum Laude(2012)

Virginia Commonwealth University
Presidential Scholarship (Full tuition, room & board) (2008)

PEER REVIEWED PUBLICATIONS

Schweer, D., Carmouche, J.J., Jupiter, D., Ball, T., Clements, J.R.
Evaluating blood loss and the effect of antiplatelet treatment in foot and ankle amputations. *J Foot Ankle Surg*, 55 (6), pp. 1210-1215; Nov 2016

Wyckoff, E., **Schweer, D.**, and G. Cua.
Advanced Lichen Sclerosus Resulting in Complete Labial Fusion and Urinary Retention in a Postmenopausal Patient

Gynecol Reprod Health. 2018; 2(4): 1-3; Aug 2018

Carbajal-Mamani SL, **Schweer D,** Markham MJ, et al. Robotic-assisted interval cytoreductive surgery in ovarian cancer: a feasibility study. *Obstet Gynecol Sci*. 2020;63(2):150-157.

Carbajal-Mamani SL, Dideban B, **Schweer D**, et al. Incidence of venous thromboembolism after robotic-assisted hysterectomy in obese patients with endometrial cancer: do we need extended prophylaxis. *J Robot Surg*. 2020

Schweer D, McCorkle JR, Rohr J, Tsodikov OV, Ueland F, Kolesar J. Mithramycin and Analogs for Overcoming Cisplatin Resistance in Ovarian Cancer. *Biomedicines.* 2021 Jan 12;9(1):70.

Schweer D, McAtee A, Neupane K, Richards C, Ueland F, Kolesar J. Tumor-Associated Macrophages and Ovarian Cancer: Implications for Therapy. *Cancers* (Basel). 2022 Apr 29;14(9):2220.

Bhosale SS, Mandal A, Hou C, McCorkle JR, **Schweer D**, Hill KS, Kolesar JM, Tsodikov OV, Rohr J, Subramanian V. Mithplatins: Mithramycin SA-Pt(II) Complex Conjugates for the Treatment of Platinum Resistant Ovarian Cancers. *ChemMedChem*. 2022 Nov 7.

Schweer, D., Anand, N., Anderson, A., McCorkle, JR., Neupane, K., Nail, A., Harvey, B., Hill, KS., Ueland, F., Richards, C., Kolesar, J. Human Macrophage-Engineered Vesicles for Utilization in Ovarian Cancer Treatment. *Frontiers in Oncology.* 2023 Jan 11.

Wei Y, Erfani S, **Schweer D**, de Gouvea R, Qadir J, Shi J, Cheng K, Wu D, Craven R, Wu Y, Olivier T, Baldwin LA, Zhou B, Zhou Y, Zhao W, Yang BB, Ueland FR, Yang XH. Targeting receptor tyrosine kinases in ovarian cancer: Genomic dysregulation, clinical evaluation of inhibitors, and potential for combinatorial therapies. *Molecular Therapeutic Oncolytics*. 2023 Feb 19

Santolaya JL, **Schweer DS**, Cardenas-Goicoechea J, Bukowski R, Santolaya-Forgas J. Bioavailability of the tumor necrosis factor alpha/regulated on activation, normal T cell expressed and secreted (RANTES) biosystem inside the gestational sac during the pre-immune stages of embryo development. *Journal of Perinatal Medicine*. 2023 Apr 18